

Journal Pre-proof

Rapid, high-temperature microwave soldering toward a high-performance cathode/
electrolyte interface

Geng Zhong, Chengwei Wang, Ruiliu Wang, Weiwei Ping, Shaomao Xu, Haiyu Qiao,
Mingjin Cui, Xizheng Wang, Yubing Zhou, Dylan Jacob Kline, Michael R. Zachariah,
Liangbing Hu

PII: S2405-8297(20)30193-8

DOI: <https://doi.org/10.1016/j.ensm.2020.05.015>

Reference: ENSM 1205

To appear in: *Energy Storage Materials*

Received Date: 9 March 2020

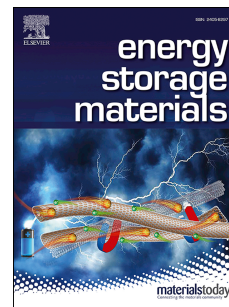
Revised Date: 14 May 2020

Accepted Date: 16 May 2020

Please cite this article as: G. Zhong, C. Wang, R. Wang, W. Ping, S. Xu, H. Qiao, M. Cui, X. Wang, Y. Zhou, D.J. Kline, M.R. Zachariah, L. Hu, Rapid, high-temperature microwave soldering toward a high-performance cathode/electrolyte interface, *Energy Storage Materials* (2020), doi: <https://doi.org/10.1016/j.ensm.2020.05.015>.

This is a PDF file of an article that has undergone enhancements after acceptance, such as the addition of a cover page and metadata, and formatting for readability, but it is not yet the definitive version of record. This version will undergo additional copyediting, typesetting and review before it is published in its final form, but we are providing this version to give early visibility of the article. Please note that, during the production process, errors may be discovered which could affect the content, and all legal disclaimers that apply to the journal pertain.

© 2020 Published by Elsevier B.V.



CRedit authorship contribution statement

Geng Zhong : Conceptualization, Methodology, Formal analysis, Resources, Software, Writing - original draft, Writing - review & editing. **Chengwei Wang**: Methodology, Formal analysis, Resources, Writing - original draft, Writing - review & editing. **Ruilu Wang**: Methodology. **Weiwei Ping**: Methodology. **Shaomao Xu**: Methodology. **Haiyu Qiao**: Formal analysis. **Mingjin Cui**: Formal analysis. **Xizheng Wang**: Formal analysis. **Yubing Zhou**: Methodology. **Dylan Jacob Kline**: Methodology. **Michael R. Zachariah**: Methodology. **Liangbing Hu**: Conceptualization, Methodology, Resources, Writing - review & editing.

Rapid, High-Temperature Microwave Soldering toward A High-Performance Cathode/Electrolyte Interface

Geng Zhong^{1a}, Chengwei Wang^{1a}, Ruiliu Wang¹, Weiwei Ping¹, Shaomao Xu¹, Haiyu Qiao¹, Mingjin Cui¹, Xizheng Wang¹, Yubing Zhou¹, Dylan Jacob Kline², Michael R. Zachariah², Liangbing Hu^{1,*}

1. Department of Materials Science and Engineering, University of Maryland, College Park, Maryland, 20742, USA
2. Department of Chemical and Environmental Engineering, University of California, Riverside, CA 92521, USA

* Email: binghu@umd.edu

^aThese authors contributed equally to this work.

Keywords: Solid-state battery, Cathode-garnet interface, Garnet electrolyte, Microwave, Rapid heating

Rapid, High-Temperature Microwave Soldering toward A High-Performance Cathode/Electrolyte Interface

Keywords: Solid-state battery, Cathode-garnet interface, Garnet electrolyte, Microwave, Rapid heating

Abstract

Solid-state lithium batteries using inorganic electrolytes are expected to revolutionize energy storage systems due to their better safety and high energy density. However, their application is greatly hindered by the poor solid-solid interface between the solid-state electrolyte (SSE) and electrodes, particularly the cathode. Herein, we report a facile strategy to address the high cathode/SSE interfacial resistance through rapid, high-temperature microwave soldering. As a proof-of-concept demonstration, we soldered a garnet-type $\text{Li}_7\text{La}_3\text{Zr}_2\text{O}_{12}$ (LLZO) SSE with a V_2O_5 cathode, which feature high thermal stability and suitable melting temperatures. Our microwave soldering technique can selectively melt the surface of the granular V_2O_5 and rapidly form an intact and continuous cathode layer with tightly embedded carbon black nanoparticles, leading to a remarkable 690-time increase of the electronic conductivity of cathode. Additionally, the melted V_2O_5 cathode is conformally soldered to the garnet electrolyte, resulting in a 28-fold decrease of the cathode/garnet interfacial resistance (from $14.4 \text{ k}\Omega\cdot\text{cm}^2$ to $0.5 \text{ k}\Omega\cdot\text{cm}^2$). As a result, this all-solid-state full cell displays a low overall resistance of $0.3 \text{ k}\Omega\cdot\text{cm}^2$ at $100 \text{ }^\circ\text{C}$, which enables stable cyclability of the battery without the addition of liquid/polymer electrolyte. The fast microwave soldering strategy constitutes a significant step towards the development of the all-solid-state batteries.

Introduction

Solid-state lithium batteries (SSLBs) are considered a promising energy storage system due to their high energy density, longer cycle life, and improved safety compared to traditional lithium ion batteries.¹ Solid-state electrolytes (SSEs) have enabled significant advances in SSLBs, with numerous materials investigated, including LIPON,^{2, 3} LISCON,^{4, 5} perovskites,^{6, 7} antiperovskites,⁸ hydrides^{9, 10} and garnet.¹¹⁻¹³ These studies have resulted in an improved bulk Li-ionic conductivity of 10 mS/cm,¹⁴ which rivals that of standard organic liquid electrolytes. Nevertheless, large-scale commercialization of SSLBs has remained challenging due to the poor solid-solid interfacial contact between the SSE and electrodes (both anode and cathode), which creates large interfacial impedance that can be more than two orders of magnitude higher than batteries with liquid or polymer electrolytes.¹⁵ Furthermore, this poor and non-conformal interfacial contact can lead to high local current density, which may cause uneven Li plating/stripping and that could ultimately short circuit the battery.^{15, 16}

Fortunately, the high electronic and Li-ion conductivity and low softening temperature (~180 °C) of the lithium metal anode provide us the opportunity to minimize the anode/SSE interfacial impedance through surface modification and interfacial engineering. For instance, by introducing a thin interphase layer between the Li anode and SSEs, the wetting interaction between them is dramatically improved, resulting in a significant decrease of interfacial resistance.¹⁷⁻²² However, the cathode interface has remained an issue hindering the development of SSLBs due to the low ionic conductivity of cathode materials and the poor contact between rigid granular cathode powders and stiff SSEs.

To date, limited approaches have been proposed to address the problem of the cathode/SSE interface, among which most involve the utilization of a new layer of Li-ion conductor. For example, a polymer Li-ion conductor was sandwiched between the cathode and SSE to cushion the poor contact at their interface.^{23, 24} The crosslinked polymer with good interfacial compatibility serves as both binder and electrolyte, which enables stable cycling of the solid-state batteries. However, the soft organic polymer may introduce potential safety concerns, as well as sacrifice the device's thermal stability and lower its energy density due to the addition of inactive materials. In response to these limitations, inorganic Li-ion conductive interlayers (e.g., $\text{Li}_4\text{Ti}_5\text{O}_{12}$,²⁵ LiBO_3 ,²⁶ $\text{Li}_{2.3}\text{C}_{0.7}\text{B}_{0.3}\text{O}_3$,²⁷ and $\text{Li}_{1.4}\text{Al}_{0.4}\text{Ti}_{1.6}(\text{PO}_4)_3$ ²⁸) have recently been employed to improve the cathode interface, for rechargeable solid-state batteries. These ceramic interlayers, which feature good thermal and chemical stability as well as high mechanical strength, can significantly improve the battery's safety.^{29, 30} By sintering them at the interface between the cathode and SSE, sufficient interfacial contact is also achieved, which leads to reduced interfacial impedance and improved electrochemical performance.²⁵⁻³⁰ However, the long sintering time (usually longer than 30 min) at high temperature not only lowers the processing efficiency but also causes side reactions that compromise the battery performance.³¹ Therefore, a facile and efficient technique is needed to improve to address the cathode interface issue in order to achieve high performance SSLBs.

In this work, we demonstrate a rapid high-temperature microwave soldering strategy that enables close binding between the cathode and SSE, leading to an improved interface with significantly decreased interfacial resistance. As a proof-of-concept demonstration, we subjected the solid-

solid interface between a V_2O_5 cathode and garnet-type LLZO SSE to this microwave soldering process, due to their high thermal stability and suitable melting temperatures. The rapid microwave heating enables the selective melting and re-solidifying of the surface of V_2O_5 within a few seconds, which results in the soldering between the cathode and SSE as well as the particles in the cathode composite. As a result, the interfacial resistance between the cathode and solid electrolyte as well as the electronic resistance of cathode composite dramatically decrease. Based on the improved cathode interface, this Li/Garnet/ V_2O_5 all solid-state battery displayed a low overall resistance and was successfully cycled over 60 cycles at 100 \square , without the introduction of other interlayer or polymer binders. This work provides a facile and effective strategy to achieve a sufficient interface between the cathode and SSE, constituting a significant step towards the development of safe and high-energy-density all-solid-state batteries.

Figure 1 shows the schematic of the rapid microwave soldering process and its effect on the cathode/SSE interface. Carbon black (CB) was mixed with V_2O_5 to improve the electronic conductivity of the cathode composite. This composite was then coated onto both sides of the garnet pellet and dried to form a symmetric cell. Due to the high stiffness of the V_2O_5 grains (Figure S1), the cathode has poor physical contact with the garnet SSE as well as carbon black (Figure 1a). We then buried this cell in a carbon-black bath, which provides a high-temperature environment when subjected to microwave irradiation (Figure 1b). Rapid soldering was enabled by two-steps in this microwave heating process, including slow preheating (500 W, 9 s) and rapid heating (1000 W, 7 s). The slow preheating can prevent the garnet pellet from cracking due to the intense temperature ramping achieved from rapid heating. During the rapid heating, the temperature of the carbon-black bath increased up to ~ 1200 K, which is much higher than the

melting temperature of V_2O_5 (~960 K). As a result, the V_2O_5 melted from surface and penetrated into the void spaces between the solid content, resulting in solid soldering between the cathode and SSE as well as the adjacent cathode particles (Figure 1c). The short soldering time can also inhibit potential side reactions that impair the SSE and cathode materials, which is essential for achieving a high-performance solid-state battery.

Journal Pre-proof

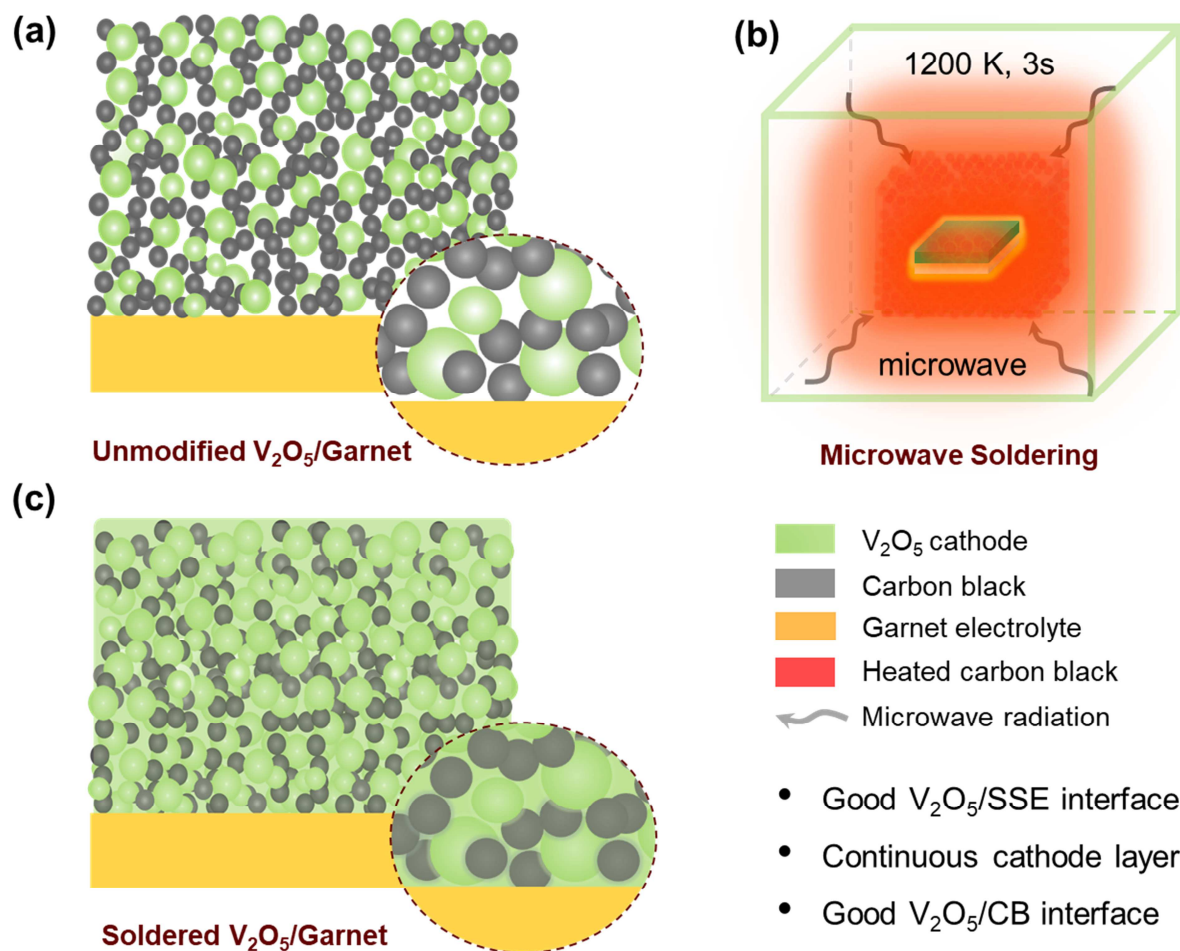


Figure 1. (a) Before microwave soldering, the rigid V_2O_5 particles are isolated with poor point-to-point contact with both the carbon black nanoparticles and SSE pellet. (b) Schematic illustration of the rapid microwave soldering process of the cathode/SSE interface. (c) The high-temperature soldering causes the V_2O_5 to melt and penetrate into void spaces, forming good interfacial contact between the carbon black and SSE.

Figure 2a shows a photo image of the microwave soldering process in which a strong light emission can be observed due to the high temperature achieved. The emission is above the black level and within the error threshold that can be captured to calculate temperature based on the black-body theory.³² Therefore, we used a high-speed camera to record the sample's color

images during the soldering treatment, which were then computer processed to provide the raw color of each pixel, enabling spatial- and time-resolved ratio pyrometry to obtain the temperature.³³ The peak temperature of the soldering process reached up to ~1200 K, which lasted for 3 s until the microwave was stopped, with a small temperature fluctuation of less than ± 30 K (Figure 2b). The subsequent cooling process under blowing air takes no more than 10 s, which makes the whole treatment less than 20 s long. As reported in our previous study, the temperature of microwave soldering can be controlled by adjusting the microwaving power or the amount of carbon black in the heating bath.³² Note that the short soldering period and stable soldering temperature is beneficial for inhibiting side reactions.

To study the effect of the microwave soldering, we first conducted a tape-testing experiment to investigate the contact between the cathode composite and garnet SSE. Specifically, the scotch tape was pasted on the cathode side and peeled off to see whether the cathode layer was remained well. Before microwave soldering, the cathode composite could be peeled off easily from the surface of the garnet, indicating insufficient interfacial contact (Figure 2c, top). In contrast, after microwave soldering, the cathode composite was bonded tightly to the garnet surface without peeling-off, demonstrating an obviously improved cathode/garnet interface (Figure 2c, bottom).

We also used scanning electron microscopy (SEM) to study the micromorphology of the interface between the V_2O_5 cathode and garnet SSE as well as the structure of cathode composite. The cross-sectional image of the unmodified cathode/SSE interface shows that the bad contact between the cathode and SSE, leaving a large interfacial gap of ~ 2 μm (Figure 2d), which

indicates a poor interface between the cathode and garnet. In addition, the V_2O_5 cathode and conductive carbon black were granularly isolated, with a loose and porous structure (Figure 2e, S2), indicating inferior physical contact within the cathode composite. However, after microwave soldering, we observed a dense cathode layer closely adhered on the garnet SSE with no noticeable gap, demonstrating significantly enhanced interfacial contact between the cathode and SSE (Figure 2f). Additionally, the top-view image shows the V_2O_5 particles melted together, forming a continuous matrix with the uniformly embedded conductive carbon black (Figure 2g, S3). Figure 2h shows the cross-sectional energy-dispersive X-ray spectroscopy (EDS) mapping of the soldered cathode/garnet interface, where La, Zr (from garnet), and V (from the cathode) elements were conformal distributed in garnet and cathode sides, further suggesting good interfacial contact between the cathode and garnet SSE.

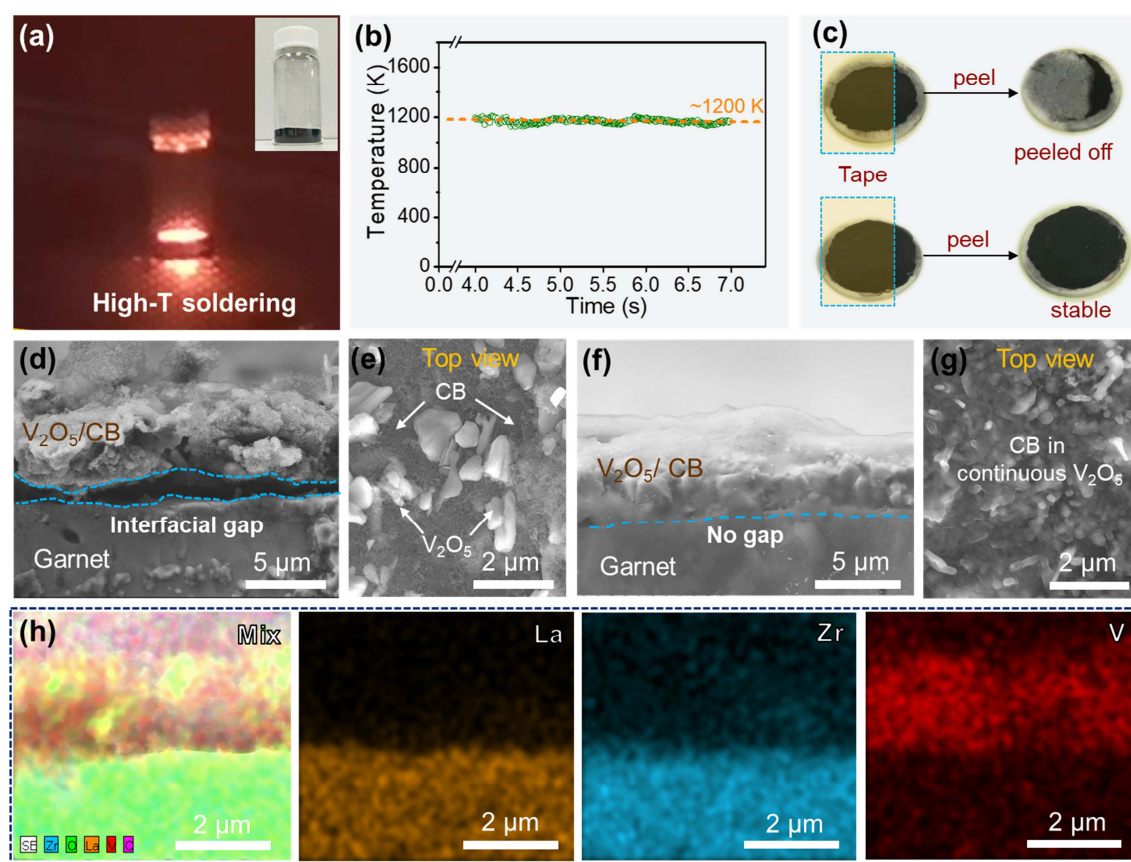


Figure 2. Characterization of the rapid microwave soldering process. (a) Photo image of the high-T soldering process. A strong light emission can be observed due to the black body radiation. Inset is the photo image of the device before high-temperature soldering. (b) The temperature profile of the microwave process, showing a stable temperature (~ 1200 K) was maintained for 3 s. (c) Photo images of the tape-testing experiment of the unmodified V_2O_5 /SSE (top) and soldered V_2O_5 /SSE (bottom). The soldering treatment results in strong contact between the V_2O_5 and SSE with no cathode detachment. (d) Cross-sectional and (e) top-view SEM images of the unmodified cathode/SSE. (f) Cross-sectional and (g) top-view SEM images of the soldered cathode/SSE. (h) EDS elemental mapping of the soldered V_2O_5 /SSE cross-section.

Besides the improved interfacial contact, it is also important to ensure there is no degradation of the cathode and SSE during the microwave soldering process. The grain size distributions of unmodified and microwave-treated garnet were calculated based on SEM images (Figure S4), which show negligible change after microwave soldering. The Raman spectra of both the unmodified and microwaved cathode/SSE half-cells feature the same main characteristic peaks of the cubic garnet phase (Figure 3a), demonstrating no phase change in the SSE during high-temperature soldering. Furthermore, the peak at ~ 160 cm^{-1} in the unmodified garnet/cathode, corresponding to common Li_2CO_3 contaminant in garnet SSE, is absent in the microwaved garnet/cathode half-cell, indicating the removal of Li_2CO_3 after the microwave soldering process (Figure 3a). X-ray diffraction (XRD) patterns also confirm that the characteristic peaks of both the garnet (PDF#80-0457) and V_2O_5 (PDF#41-1426) are well preserved. The broaden of the garnet peaks are likely due to the lattice strain during the high temperature treatment³⁴, which

causes no degradation of Li^+ conductivity as demonstrated later. Moreover, the two obvious peaks of Li_2CO_3 (PDF#22-1141) are not present after microwave soldering (Figure 3b). The cleaning effect is also indicated by the morphology change of the garnet before and after microwave soldering (Fig. S4). The surface of the unmodified garnet was rough and covered with a layer of contamination (Figure. S4a, b), typically Li_2CO_3 ,^{27, 35, 36} which disappeared after microwave soldering, revealing a clean and smooth garnet surface (Figure S4c, d). The contact angle between Li anode and Li_2CO_3 , simulated by density functional theory (DFT), is as high as 142° , meaning a bad wettability between them. In addition, the Li_2CO_3 contamination features a low Li^+ conductivity (10^{-7} S/cm at 25°C) and a low decomposition voltage (3.2 V). In this way, the removal of Li_2CO_3 is beneficial for realizing a higher ionic conductivity and good stability for garnet SSE as well as better wettability with the lithium metal anode.³⁷⁻³⁹

We measured the I-V curves of the cathode layer using the four-probe method to study the effect of soldering treatment on the electronic conductivity of cathode composite. Based on the I-V curves (Figure 3c), the unmodified cathode exhibits a conductivity of 0.0016 S/cm, which dramatically increases to 1.1 S/cm after soldering treatment, corresponding to a 690-fold improvement. We attribute the improved conductivity of the cathode composite to the continuous V_2O_5 and tightly embedded nanograined carbon black (Figure S3). The high electronic conductivity benefits the charge transfer of the electrode, which can lead to better electrochemical performance.⁴⁰⁻⁴² Additionally, we used electrochemical impedance spectroscopy (EIS) to study the resistance of the garnet itself and cathode/garnet interface. The bulk resistance of the unmodified garnet was first evaluated with a lithium electrode, following our previous method,⁴³ resulting in values of 160, 62, 23, and $13 \Omega\cdot\text{cm}^2$ at 25, 50, 75, and 100°C ,

respectively, corresponding to ionic conductivities of 2.9×10^{-4} , 7.4×10^{-4} , 2.0×10^{-3} , and 3.5×10^{-3} S/cm (Figure S5). As shown in Figure 3d, the overall resistance from the electrolyte and interfaces before soldering was $29.0 \text{ k}\Omega\cdot\text{cm}^2$ at $25 \text{ }^\circ\text{C}$, therefore we calculated the interface resistance to be as high as $14.4 \text{ k}\Omega\cdot\text{cm}^2$ (interfacial resistance = (overall resistance-bulk resistance)/2). After microwave soldering, the interfacial resistance dramatically decreased to $0.5 \text{ k}\Omega\cdot\text{cm}^2$, corresponding to a more than 28-times decrease. Note that the ionic conductivity of the garnet itself showed only a slight increase of less than 0.2-fold after an identical microwave treatment, as evidenced by the EIS results (Figure S6). Therefore, we can attribute the decrease of the all-solid-state cathode/electrolyte interfacial resistance to the improved contact after microwave soldering. In addition, the diffusion impedance decreases significantly after microwave soldering, which is likely due to the conformal interconnection within the cathode layer (Figure S3).

Due to the excellent thermal stability of both the electrode and electrolyte, one promising application of this solid-state battery lies in high-temperature energy storage systems,^{44,45} such as thermal battery used in geothermal boreholes.⁴⁶ Therefore, we also conducted EIS of the microwave-soldered symmetric cell at increased temperatures of 50 , 75 , $100 \text{ }^\circ\text{C}$, which show distinct differences from that of $25 \text{ }^\circ\text{C}$. Based on these spectra (Figure 3e), we calculated the cathode/electrolyte interfacial resistance to be 115 , 66 , and $26 \text{ }\Omega\cdot\text{cm}^2$ at 50 , 75 , and $100 \text{ }^\circ\text{C}$, respectively (Figure 3f). Therefore, the high temperature can further facilitate the interfacial charge transfer, thus leading to fast interfacial reaction kinetics in the solid-state battery. Note that the microwave soldering technique is typically a melting-solidification process under high temperature which is also a common transformation process in other material. Therefore, it

shows great potential in welding other cathode materials with garnet SSE, especially those who exhibit good thermal stability (e.g. LiFePO_4).

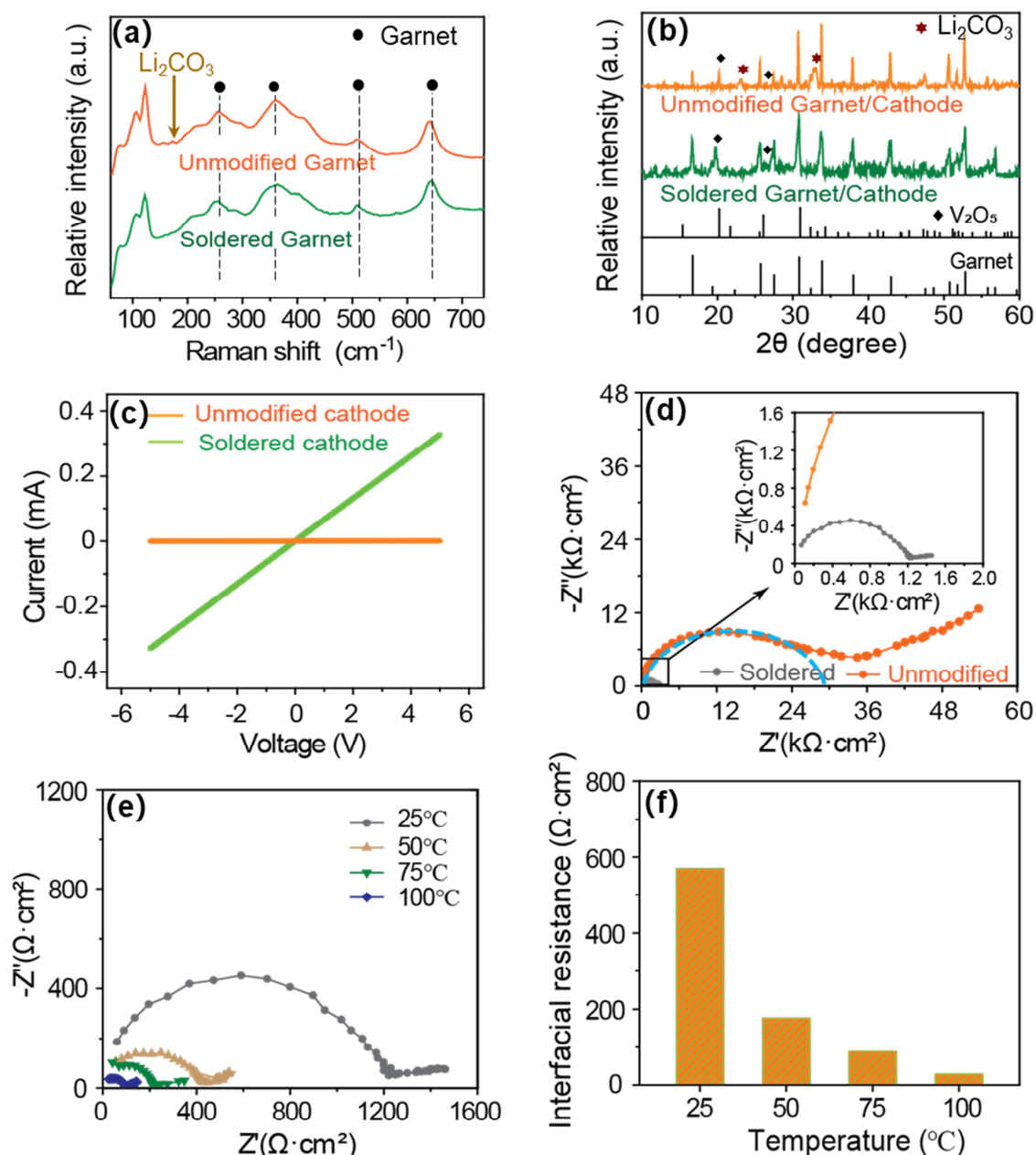


Figure 3. Characterization of the cathode/SSE/cathode symmetric cells, using garnet SSE and V_2O_5 /carbon black composite electrodes. (a) Raman spectroscopy and (b) XRD patterns of the unmodified and microwave (MW) soldered symmetric cells. (c) I-V curves of the cathode layers

and (d) an EIS plot of the unmodified and microwave-soldered symmetric cells. (e) The EIS and (f) calculated interfacial resistance of the symmetric cell after microwave soldering at temperatures of 25, 50, 75, and 100 °C.

To demonstrate the potential applications of this improved interface, we assembled an all solid-state battery by melting the lithium anode onto the electrolyte side of the microwave-soldered cathode/garnet half-cell (Figure 4a). Figure 4b shows the EIS plots of the resulting battery, in which the overall resistance displays a remarkable drop as the temperature increases. When elevating the temperature from 25 to 100 °C, the resistance from the electrolyte and interfaces decreased by 9-fold, from $\sim 490 \text{ } \Omega \cdot \text{cm}^2$ to $\sim 54 \text{ } \Omega \cdot \text{cm}^2$. Meanwhile, compared to the unmodified cathode/garnet cell, the overall resistance of the battery after soldering significantly decreased at all testing temperatures (Figure 4c, S7). Since the garnet pellets, electrodes and the anode/garnet interfaces in the two cases are almost identical, the dramatically decreased overall resistances can be attributed to the improved cathode/garnet interface.

Due to this improved interface, the all solid-state battery can cycle effectively between $\sim 1\text{--}4.2 \text{ V}$ at 100 °C. Figure 4d shows the initial charge/discharge curves of the batteries with the unmodified and microwave-soldered cathode/garnet interface at a current density of 116 mA/g. The battery with the soldered interface exhibits a significantly prolonged charge/discharge time (~ 15 -fold, Figure 4e), which means a much higher specific capacity due to the improved cathode/garnet property. Additionally, the magnified voltage profiles showed distinct plateaus with a small overpotential for the soldered cell when compared to the battery with the unmodified cathode/garnet interface, indicating a remarkably reduced electrochemical polarization. (Figure S8).

To further study the cycling performance and rate performance, the soldered solid-state battery was cycled at 100 °C under various current densities. When cycled at 116 mA/g, the discharge capacity of the first cycle was ~114 mAh/g, which stabilized to ~80 mAh/g in the following 20 cycles (Figure 4f). Even at 174, 232, and 290 mA/g, the discharge capacity can reach 70, 60, and 48 mAh/g, respectively. When recovering the current density back to 116 mA/g, the discharge capacity returns to ~78 mAh/g, demonstrating the superior stability of the soldered cathode/garnet interface. The coulombic efficiency exceeded 90% at all the current densities suggesting a good reversibility of the soldered battery. In addition, after cycling, the EIS plots of the battery show negligible increase in overall resistance (Figure 4g). These results indicate that the solid-state battery Li/SSE/V₂O₅ featuring the microwave-soldered cathode interface exhibits superior electrochemical stability.

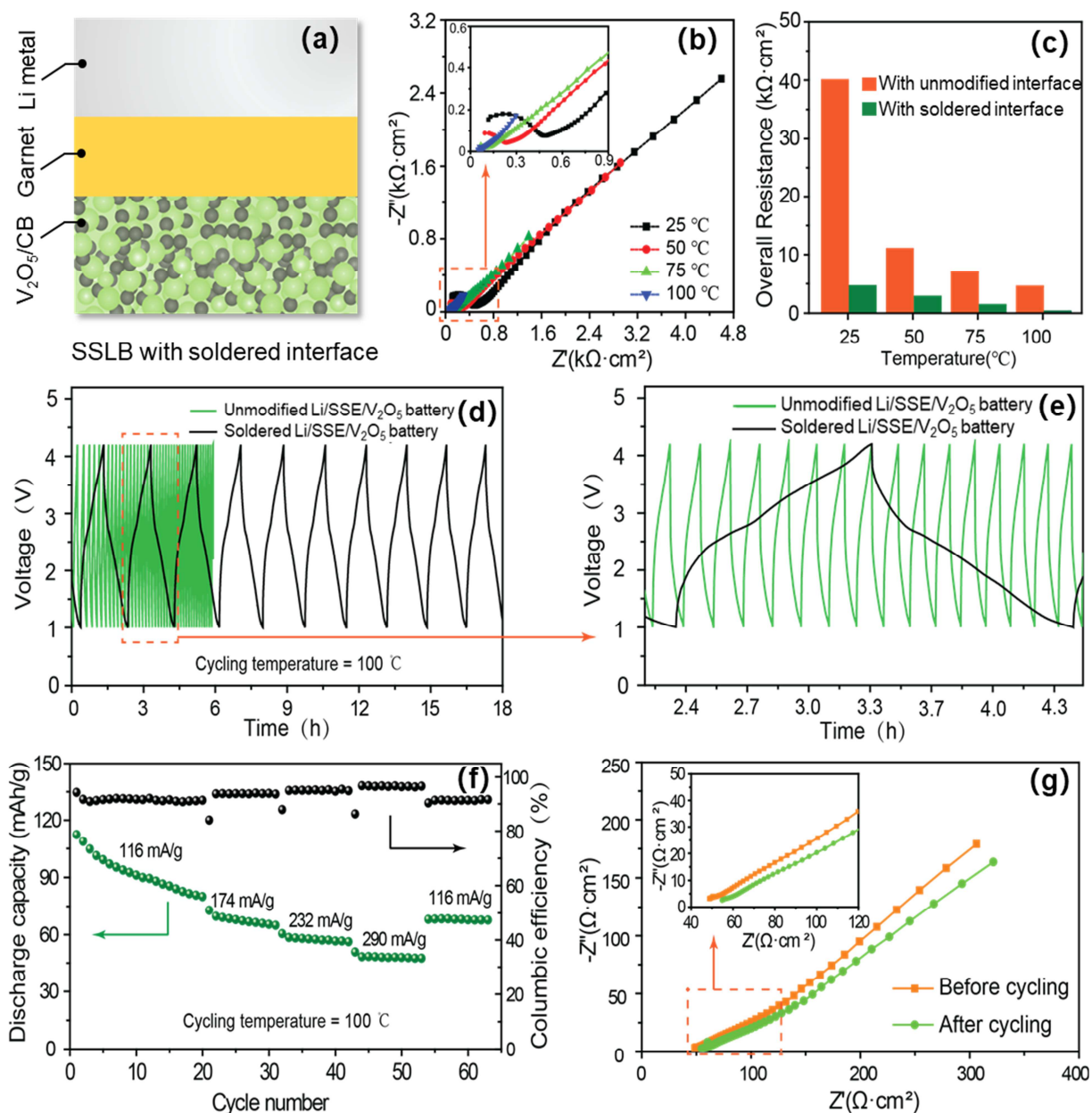


Figure 4. Characterization of the all-solid-state full cells. The cathode/garnet interface was microwave-soldered before assembling. (a) Schematic illustration of the all-solid-state full cell, using garnet electrolyte, the V_2O_5 /carbon black composite cathode, and a lithium metal anode. (b) EIS and (c) comparison of overall resistance of the Li/SSE/ V_2O_5 cells (with unmodified or soldered cathode interfaces) tested at temperatures of 25, 50, 75, and 100 °C. (d)

Discharge/charge curves for the batteries featuring the unmodified and soldered cathode interfaces. (e) Magnified view of a certain region of (d). (f) The discharge capacity and coulombic efficiency of the Li/SSE/V₂O₅ battery with the microwave-soldered cathode interface, cycled at 100 °C. (g) EIS of the microwave-soldered cell, before and after cycling.

Conclusion

In summary, we reported a rapid microwave soldering strategy for overcoming the large solid-solid interfacial resistance between the cathode and ceramic electrolyte. The high-temperature microwave heating enables the fast melting/solidifying of the cathode to produce good interfacial contact with SSE, while the short soldering duration inhibits detrimental side reactions. The high-temperature soldering process can also boost the electronic conductivity of the cathode composites, which is important to improve the performance of the battery. As a demonstration, we used this strategy to achieve conformal contact between a V₂O₅ cathode and garnet solid-state electrolyte, as well as close interconnection between the particles in the cathode composite, which lead to significantly reduced interfacial impedance and cathode resistance. As a result of these advantages, the all-solid-state Li/Garnet/V₂O₅ battery based on the microwave-soldered cathode interface displayed an overall resistance as low as 0.3 kΩ·cm² at 100 °C and exhibited a superior electrochemical performance, with a discharge capacity of 80 mAh/g when cycled at 116 mA/g for 20 cycles and 48 mAh/g when cycled at 290 mA/g for 10 cycles. We note this microwave soldering method is not limited to V₂O₅ and garnet but can be extended to other cathode and electrolyte systems with suitable melting temperature, thus providing a promising strategy for the practical application of an all-solid-state battery.

Experiments

Assembly of the cells.

The garnet SSE was synthesized by following a previous method without Al doping.³⁷ The cathode/garnet/cathode symmetric cell was fabricated by a simple dip coating method. Typically, a mixture of V₂O₅ powders (99.6%, Sigma-Aldrich) and carbon black with mass ratio of 86:14 were ground in a mortar for 30 min before being dispersed into N-methyl-2-pyrrolidone (>99.7%, Sigma-Aldrich) to form a 20 mg/mL cathode dispersion. Then, the cathode dispersion was dip-coated onto both side of a freshly polished garnet pellet, followed by drying in a 60 °C oven for 5 h. The mass loading of the cathode composite was controlled to be ~2 mg/cm², ~5 μm. The Li/garnet/Li symmetric cell was fabricated in an Ar-filled glovebox by smearing molten Li onto both sides of the freshly polished garnet, during which a small amount of Sn was mixed with Li (the mass ratio of Sn to Li was ~1/4) to minimize the Li/garnet interfacial impedance, following a previous work.³⁸ The all solid-state battery was assembled by similarly smearing the molten lithium on to the garnet side of the cathode/garnet half-cell.

Rapid microwave soldering.

The as-prepared cells were buried into a bath of carbon black (Ketjen black EC-600JD, 160 mg) in a vial, which was then directly placed in a domestic microwave oven (Panasonic, NN-H965BFX). Here, carbon black serves as a heating source to provide a high-temperature environment for the rapid soldering when subjected to a two-step microwave radiation process. Specifically, 500 W microwave radiation was first applied for 9 s to preheat the sample, during which the temperature was <1000 K, as no light emission was observed in this process.⁴⁷ After that, 7 s of 1000 W microwave radiation was immediately applied to generate high temperature

(~1200 K) for the rapid soldering. The temperature of the soldering process was evaluated, following a previous method^{32, 33} by fitting the spectrum of the light emission with black-body radiation equation, which was captured by a high-speed camera (Vision Research Phantom Miro M110). As technique relies on the visible light emission (typically >1000 K) from black-body radiation, we measured the peak temperature of the soldering process, which occurred in the last 3 s of microwave radiation.

Materials characterization

The morphologies and elemental mapping were examined on a field-emission SEM (Hitachi SU-70). The XRD patterns were obtained on a D8 Advance system (Bruker AXS, WI) using Cu K α radiation. Raman characterization was conducted on a Horiba Jobin Yvon using a 532 nm solid-state laser with a 4 s integration time for 4 repeated measurements. The I-V curve was measured with a typical four-point probe method using a Keithley 2400 as the power supply unit.

Electrochemical characterization

Electrochemical performance was tested on a Bio-Logic potentiostat. The EIS plots were tested with 20 mV AC amplitude in the frequency from 0.1 Hz to 1 MHz. The cycling measurement was conducted at current densities from 116 mA/g to 290 mA/g, with a voltage of ~1.0–4.2 V. All the electrochemical tests were carried out in an Ar-filled glovebox with a box furnace to control the testing temperature.

Reference:

- (1) Manthiram, A.; Yu, X.; Wang, S., Lithium battery chemistries enabled by solid-state electrolytes. *Nat. Rev. Mater.* **2017**, *2*, 1.
- (2) Kozen, A. C.; Pearse, A. J.; Lin, C.-F.; Noked, M.; Rubloff, G. W., Atomic layer deposition of the solid electrolyte LiPON. *Chem. Mater.* **2015**, *27*, 5324.
- (3) Lacivita, V.; Westover, A. S.; Kercher, A.; Phillip, N. D.; Yang, G.; Veith, G.; Ceder, G.; Dudney, N. J., Resolving the amorphous structure of lithium phosphorus oxynitride (Lipon). *J. Am. Chem. Soc.* **2018**, *140*, 11029.
- (4) Xu, X.; Takada, K.; Watanabe, K.; Sakaguchi, I.; Akatsuka, K.; Hang, B. T.; Ohnishi, T.; Sasaki, T., Self-organized core-shell structure for high-power electrode in solid-state lithium batteries. *Chem. Mater.* **2011**, *23*, 3798.
- (5) Chen, R.; Qu, W.; Guo, X.; Li, L.; Wu, F., The pursuit of solid-state electrolytes for lithium batteries: from comprehensive insight to emerging horizons. *Mater. Horiz.* **2016**, *3*, 487.
- (6) Vicente, N.; Garcia - Belmonte, G., Organohalide perovskites are fast ionic conductors. *Adv. Energy Mater.* **2017**, *7*, 1700710.
- (7) Kawai, H.; Kuwano, J., Lithium Ion Conductivity of A - Site Deficient Perovskite Solid Solution $\text{La}_{0.67-x}\text{Li}_{3x}\text{TiO}_3$. *J. Electrochem. Soc.* **1994**, *141*, L78.
- (8) Li, Y.; Zhou, W.; Xin, S.; Li, S.; Zhu, J.; Lü, X.; Cui, Z.; Jia, Q.; Zhou, J.; Zhao, Y., Fluorine-doped Antiperovskite electrolyte for all-solid-state lithium-ion batteries. *Angew. Chem. Int. Ed.* **2016**, *55*, 9965.
- (9) Mohtadi, R.; Remhof, A.; Jena, P., Complex metal borohydrides: multifunctional materials for energy storage and conversion. *Condens. Matter* **2016**, *28*, 353001.
- (10) Matsuo, M.; Remhof, A.; Martelli, P.; Caputo, R.; Ernst, M.; Miura, Y.; Sato, T.; Oguchi, H.; Maekawa, H.; Takamura, H., Complex hydrides with $(\text{BH}_4)^-$ and $(\text{NH}_2)^-$ anions as new lithium fast-ion conductors. *J. Am. Chem. Soc.* **2009**, *131*, 16389.
- (11) Huang Y.; Chen B.; Duan J.; Yang F.; Wang T.; Wang Z.; Yang W.; Hu C.; Luo W.; Huang Y., g-C₃N₄: An Interface Enabler for Solid-State Lithium Metal Batteries. *Angew. Chem. Int. Ed.* **2019**.
- (12) Murugan, R.; Thangadurai, V.; Weppner, W., Fast lithium ion conduction in garnet-type $\text{Li}_7\text{La}_3\text{Zr}_2\text{O}_{12}$. *Angew. Chem. Int. Ed.* **2007**, *46*, 7778.
- (13) Li, Y.; Han, J.-T.; Wang, C.-A.; Xie, H.; Goodenough, J. B., Optimizing Li^+ conductivity in a garnet framework. *J. Mater. Chem.* **2012**, *22*, 15357.
- (14) Kamaya, N.; Homma, K.; Yamakawa, Y.; Hirayama, M.; Kanno, R.; Yonemura, M.; Kamiyama, T.; Kato, Y.; Hama, S.; Kawamoto, K., A lithium superionic conductor. *Nat. Mater.* **2011**, *10*, 682.
- (15) Dai, J.; Yang, C.; Wang, C.; Pastel, G.; Hu, L., Interface engineering for garnet-based solid-state lithium-metal batteries: Materials, structures, and characterization. *Adv. Mater.* **2018**, *30*, 1802068.
- (16) Santosh, K.; Longo, R. C.; Xiong, K.; Cho, K., Electrode-electrolyte interface for solid state Li-ion batteries: point defects and mechanical strain. *J. Electrochem. Soc.* **2014**, *161*, F3104.

- (17) Han, X.; Gong, Y.; Fu, K. K.; He, X.; Hitz, G. T.; Dai, J.; Pearse, A.; Liu, B.; Wang, H.; Rubloff, G.; Mo Y.; Thangadurai V.; Wachsman E. D.; Hu L., Negating interfacial impedance in garnet-based solid-state Li metal batteries. *Nat. Mater.* **2017**, *16*, 572.
- (18) Li, Y.; Zhou, W.; Chen, X.; Lü, X.; Cui, Z.; Xin, S.; Xue, L.; Jia, Q.; Goodenough, J. B., Mastering the interface for advanced all-solid-state lithium rechargeable batteries. *Proc. Natl. Acad. Sci.* **2016**, *113*, 13313.
- (19) Shao, Y.; Wang, H.; Gong, Z.; Wang, D.; Zheng, B.; Zhu, J.; Lu, Y.; Hu, Y.-S.; Guo, X.; Li, H., Drawing a soft interface: an effective interfacial modification strategy for garnet-type solid-state Li batteries. *ACS Energy Lett.* **2018**, *3*, 1212.
- (20) He, M.; Cui, Z.; Chen, C.; Li, Y.; Guo, X., Formation of self-limited, stable and conductive interfaces between garnet electrolytes and lithium anodes for reversible lithium cycling in solid-state batteries. *J. Mater. Chem. A* **2018**, *6*, 11463.
- (21) Duan, J.; Wu, W.; Nolan, A. M.; Wang, T.; Wen, J.; Hu, C.; Mo, Y.; Luo, W.; Huang, Y., Lithium-Graphite Paste: An Interface Compatible Anode for Solid-State Batteries. *Adv. Mater.* **2019**, *31*, 1807243.
- (22) Ruan, Y.; Lu, Y.; Huang, X.; Su, J.; Sun, C.; Jin, J.; Wen, Z., Acid induced conversion towards a robust and lithiophilic interface for Li–Li₇La₃Zr₂O₁₂ solid-state batteries. *J. Mater. Chem. A* **2019**, *7*, 14565.
- (23) Li, Y.; Xu, B.; Xu, H.; Duan, H.; Lü, X.; Xin, S.; Zhou, W.; Xue, L.; Fu, G.; Manthiram, A., Hybrid polymer/garnet electrolyte with a small interfacial resistance for lithium-ion batteries. *Angew. Chem. Int. Ed.* **2017**, *56*, 753.
- (24) Zhou, W.; Wang, S.; Li, Y.; Xin, S.; Manthiram, A.; Goodenough, J. B., Plating a dendrite-free lithium anode with a polymer/ceramic/polymer sandwich electrolyte. *J. Am. Chem. Soc.* **2016**, *138*, 9385.
- (25) Ohta, N.; Takada, K.; Zhang, L.; Ma, R.; Osada, M.; Sasaki, T., Enhancement of the high-rate capability of solid-state lithium batteries by nanoscale interfacial modification. *Adv. Mater.* **2006**, *18*, 2226.
- (26) Park, K.; Yu, B.-C.; Jung, J.-W.; Li, Y.; Zhou, W.; Gao, H.; Son, S.; Goodenough, J. B., Electrochemical nature of the cathode interface for a solid-state lithium-ion battery: interface between LiCoO₂ and garnet-Li₇La₃Zr₂O₁₂. *Chem. Mater.* **2016**, *28*, 8051.
- (27) Han, F.; Yue, J.; Chen, C.; Zhao, N.; Fan, X.; Ma, Z.; Gao, T.; Wang, F.; Guo, X.; Wang, C., Interphase engineering enabled all-ceramic lithium battery. *Joule* **2018**, *2*, 497.
- (28) Liang, J.-Y.; Zeng, X.-X.; Zhang, X.-D.; Wang, P.-F.; Ma, J.-Y.; Yin, Y.-X.; Wu, X.-W.; Guo, Y.-G.; Wan, L.-J., Mitigating interfacial potential drop of cathode–solid electrolyte via ionic conductor Layer to enhance interface dynamics for solid batteries. *J. Am. Chem. Soc.* **2018**, *140*, 6767.
- (29) Du, M.; Liao, K.; Lu, Q.; Shao, Z., Recent advances in the interface engineering of solid-state Li-ion batteries with artificial buffer layers: challenges, materials, construction, and characterization. *Energy Environ. Sci.* **2019**, *12*, 1780.
- (30) Wang, D.; Sun, Q.; Luo, J.; Liang, J.; Sun, Y.; Li, R.; Adair, K.; Zhang, L.; Yang, R.; Lu, S., Mitigating the interfacial degradation in cathodes for high-performance oxide-based solid-state lithium batteries. *ACS Appl. Mater. Inter.* **2019**, *11*, 4954.
- (31) Sakuda, A.; Hayashi, A.; Tatsumisago, M., Sulfide solid electrolyte with favorable mechanical property for all-solid-state lithium battery. *Sci. Rep.* **2013**, *3*, 2261.

- (32) Zhong, G.; Xu, S.; Cui, M.; Dong, Q.; Wang, X.; Xia, Q.; Gao, J.; Pei, Y.; Qiao, Y.; Pastel, G.; Sunaoshi T.; Yang B.; Hu L., Rapid, High-Temperature, In Situ Microwave Synthesis of Bulk Nanocatalysts. *Small* **2019**, *15*, 1904881.
- (33) Jacob, R. J.; Kline, D. J.; Zachariah, M. R., High speed 2-dimensional temperature measurements of nanothermite composites: Probing thermal vs. Gas generation effects. *J. Appl. Phys.* **2018**, *123*, 115902.
- (34) Sen, S. K.; Paul, T. C.; Dutta, S.; Hossain, M.; Mia, M., XRD peak profile and optical properties analysis of Ag-doped h-MoO₃ nanorods synthesized via hydrothermal method. *J. Mater. Sci.-Mater. El.* **2020**, *31*, 1768-1786.
- (35) Cheng, L.; Crumlin, E. J.; Chen, W.; Qiao, R.; Hou, H.; Lux, S. F.; Zorba, V.; Russo, R.; KostECKI, R.; Liu, Z., The origin of high electrolyte–electrode interfacial resistances in lithium cells containing garnet type solid electrolytes. *Phys. Chem. Chem. Phys.* **2014**, *16*, 18294.
- (36) Sharafi, A.; Yu, S.; Naguib, M.; Lee, M.; Ma, C.; Meyer, H. M.; Nanda, J.; Chi, M.; Siegel, D. J.; Sakamoto, J., Impact of air exposure and surface chemistry on Li–Li₇La₃Zr₂O₁₂ interfacial resistance. *J. Mater. Chem. A* **2017**, *5*, 13475.
- (37) Wang, C.; Xie, H.; Ping, W.; Dai, J.; Feng, G.; Yao, Y.; He, S.; Weaver, J.; Wang, H.; Gaskell, K.; Hu L., A general, highly efficient, high temperature thermal pulse toward high performance solid state electrolyte. *Energy Storage Mater.* **2019**, *17*, 234.
- (38) Li, Y.; Chen, X.; Dolocan, A.; Cui, Z.; Xin, S.; Xue, L.; Xu, H.; Park, K.; Goodenough, J. B., Garnet electrolyte with an ultralow interfacial resistance for Li-metal batteries. *J. Am. Chem. Soc.* **2018**, *140*, 6448.
- (39) Li, Y.; Chen, X.; Dolocan, A.; Cui, Z.; Xin, S.; Xue, L.; Xu, H.; Park, K.; Goodenough, J. B., Garnet electrolyte with an ultralow interfacial resistance for Li-metal batteries. *Nano Energy* **2019**, *61*, 119.
- (40) Liu, B.; Fu, K.; Gong, Y.; Yang, C.; Yao, Y.; Wang, Y.; Wang, C.; Kuang, Y.; Pastel, G.; Xie, H., Wachsman E. D.; Hu L., Rapid thermal annealing of cathode-garnet interface toward high-temperature solid state batteries. *Nano Lett.* **2017**, *17*, 4917.
- (41) Wang, C.; Zhang, L.; Xie, H.; Pastel, G.; Dai, J.; Gong, Y.; Liu, B.; Wachsman, E. D.; Hu, L., Mixed ionic-electronic conductor enabled effective cathode-electrolyte interface in all solid state batteries. *Nano energy* **2018**, *50*, 393.
- (42) Jung, H.-G.; Myung, S.-T.; Yoon, C. S.; Amine, K.; Scrosati, B.; Sun, Y.-K. In Microscale Spherical Carbon-Coated Li₄Ti₅O₁₂ as High Power Anode Material for Lithium Batteries, Meeting Abstracts, The Electrochemical Society: 2011, pp 594.
- (43) Wang, C.; Xie, H.; Zhang, L.; Gong, Y.; Pastel, G.; Dai, J.; Liu, B.; Wachsman, E. D.; Hu, L., Universal soldering of lithium and sodium alloys on various substrates for batteries. *Adv. Energy Mater.* **2018**, *8*, 1701963.
- (44) Robertson, A.; West, A.; Ritchie, A., Review of crystalline lithium-ion conductors suitable for high temperature battery applications. *Solid State Ionics* **1997**, *104*, 1.
- (45) Kato, Y.; Hori, S.; Saito, T.; Suzuki, K.; Hirayama, M.; Mitsui, A.; Yonemura, M.; Iba, H.; Kanno, R., High-power all-solid-state batteries using sulfide superionic conductors. *Nat. Energy* **2016**, *1*, 1.
- (46) Niu, Y.; Wu, Z.; Du, J.; Duan, W., A new thermal battery for powering borehole equipment: The discharge performance of Li–Mg–B alloy/LiNO₃–KNO₃/MnO₂ cells at high temperatures. *J. Power Sources* **2014**, *245*, 537.

- (47) Panagiotou, T.; Levendis, Y.; Delichatsios, M., Measurements of particle flame temperatures using three-color optical pyrometry. *Combust. Flame* **1996**, *104*, 272.

Acknowledgements

We acknowledge the support of the Maryland Nanocenter, its Surface Analysis Center and AIMLab.

Author contributions

L. Hu, G. Zhong, and C. Wang designed the experiments. G. Zhong conducted the microwave soldering experiments. C. Wang, R. Wang, and W. Ping synthesized the garnet electrolyte. G. Zhong, R. Wang, and W. Ping carried out the electrochemical characterization and analysis. H. Qiao, M. Cui, and Y. Zhou performed the material characterization. X. Wang, D. J. Kline, and M. R. Zachariah contributed to the temperature measurement. G. Zhong, C. Wang, and L. Hu collectively analyzed the data and wrote the paper.

Supporting Information for

Rapid, High-Temperature Microwave Soldering toward a High-Performance Cathode/SSE Interface

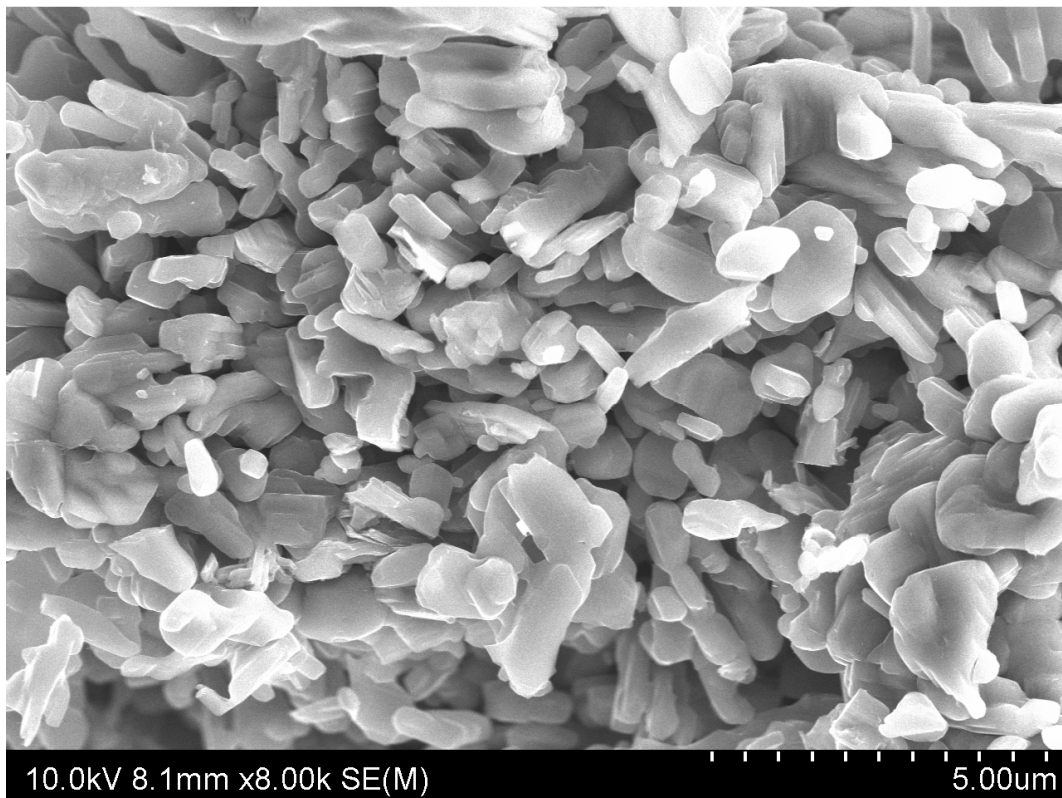


Figure S1. SEM image of V₂O₅. The high stiffness of the V₂O₅ grains at room temperature is adverse to forming good contact with the garnet SSE or carbon black.

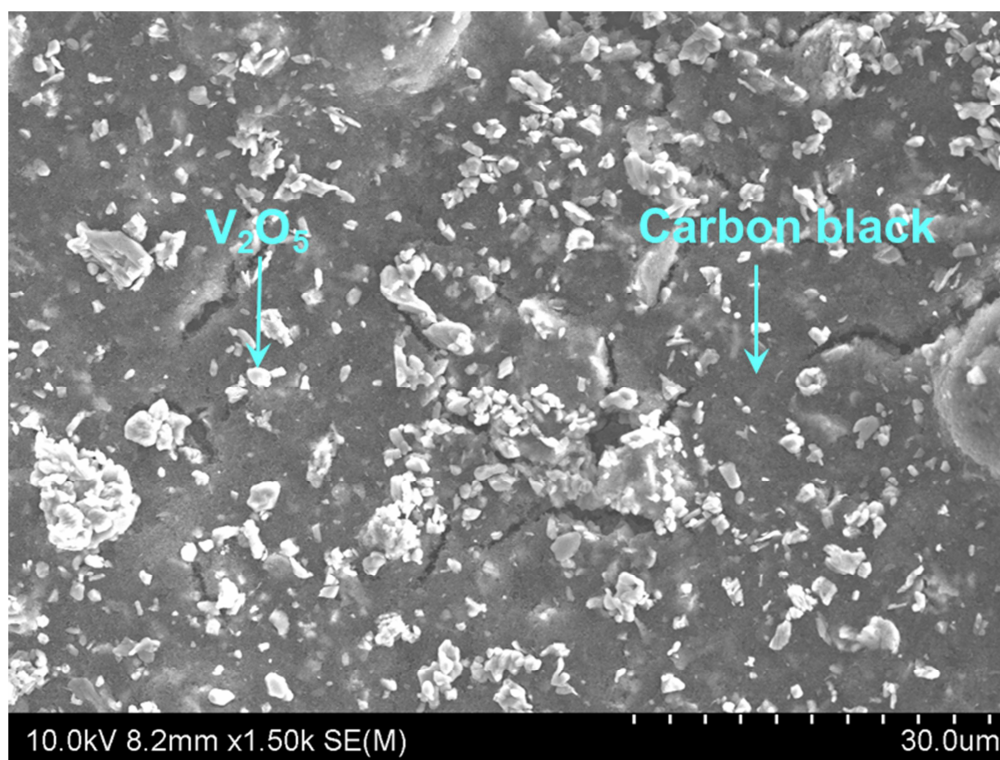


Figure S2. SEM image of unmodified cathode composite layer, in which the cathode V_2O_5 and conductive carbon black are granularly isolated with a loose and porous structure.

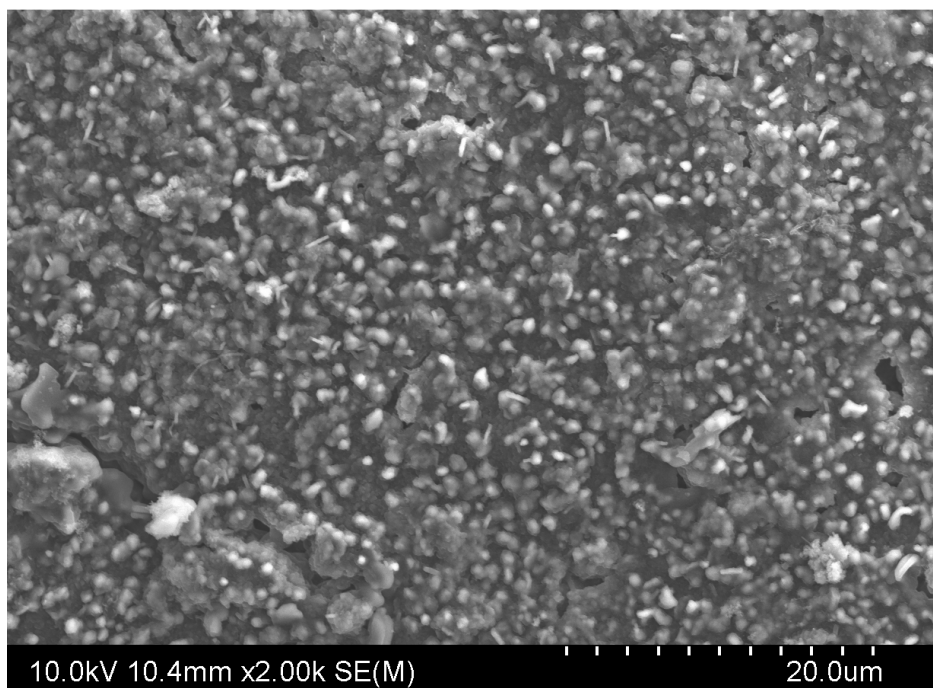


Figure S3. SEM image of the soldered cathode composite layer, in which the V_2O_5 particles are melted together, forming a continuous matrix, with the conductive carbon black uniformly embedded within.

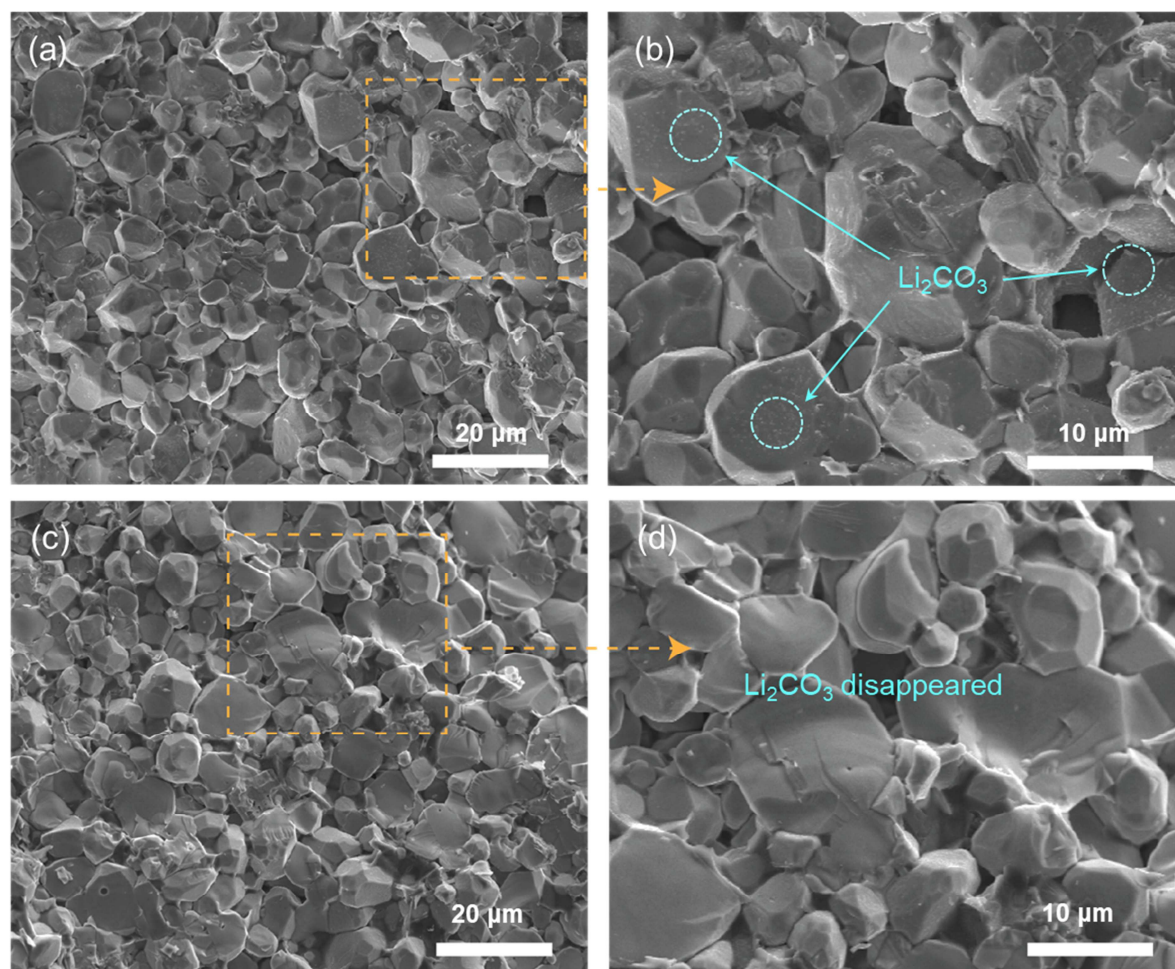


Figure S4. The cross-section SEM images of the (a, b) unmodified and (c, d) soldered garnet. The cross-section of the unmodified garnet is rough and covered with a layer of contamination, which disappeared after microwave soldering, revealing a clean and smooth garnet surface.

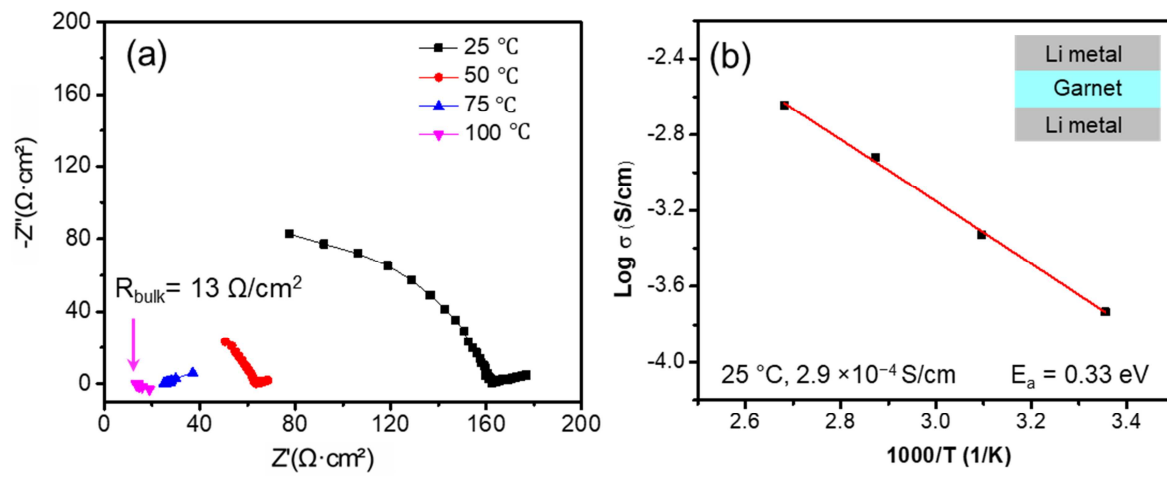


Figure S5. a. EIS of the Li/Garnet/Li cell at temperatures ranging from 25–100 °C. b. Arrhenius plot of the garnet ionic conductivity.

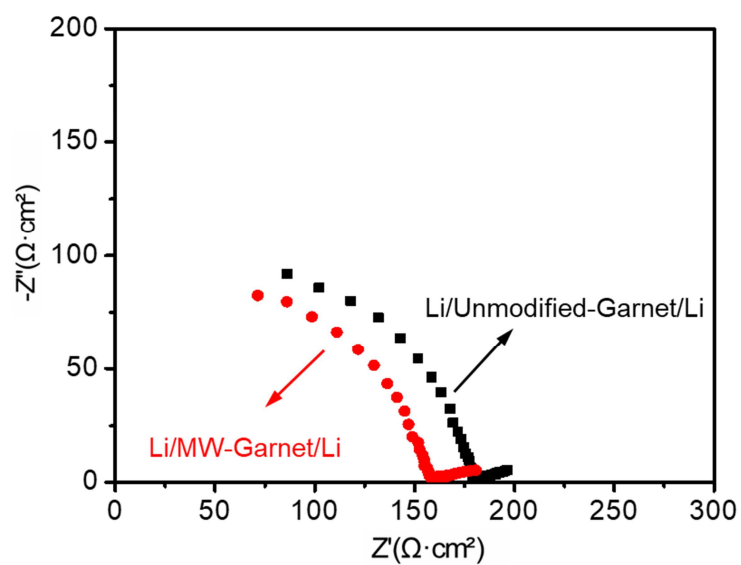


Figure S6. EIS of the Li/Garnet/Li symmetric cell using the unmodified garnet and microwave (MW)-treated garnet, which show only a slight increase in resistance.

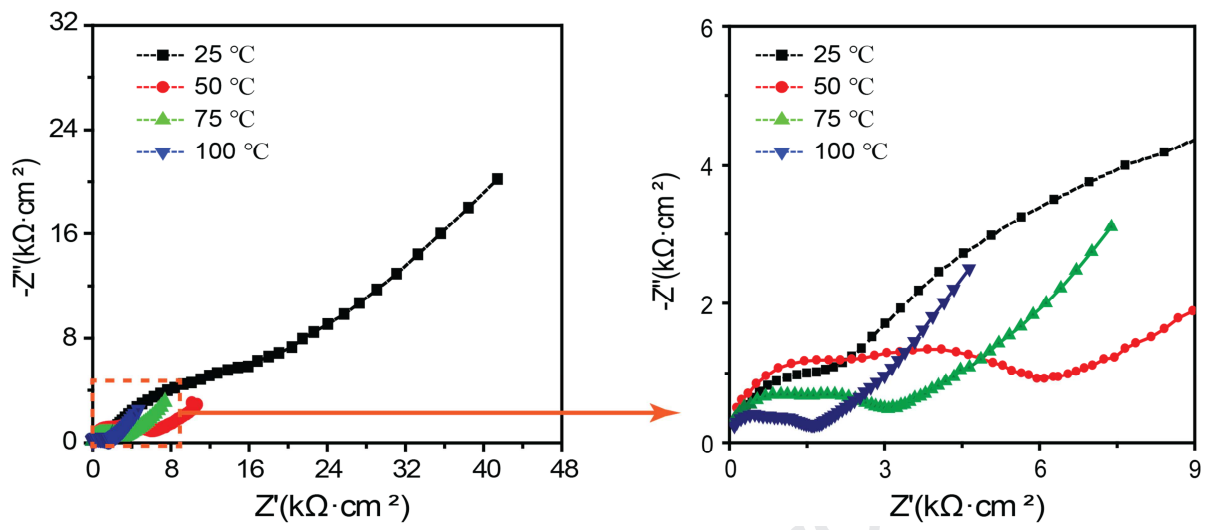


Figure S7. EIS of the all solid-state battery based on the unmodified cathode/garnet interface.

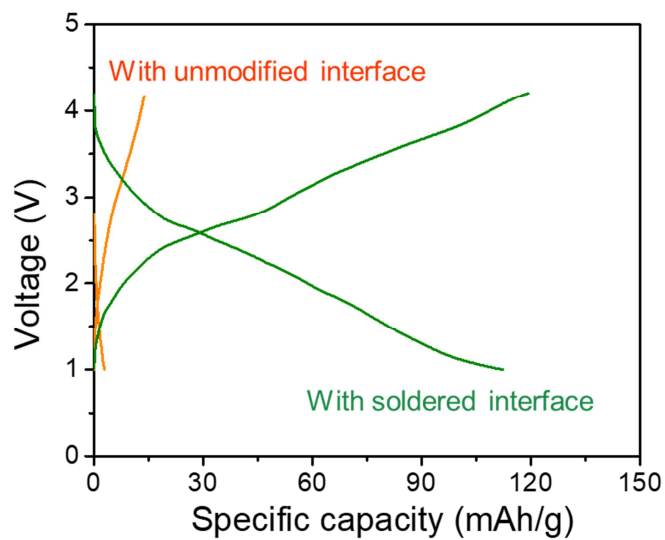


Figure S8. The voltage profiles of the first cycle of the all solid-state batteries. The battery based on the soldered cathode/garnet interface shows distinct plateaus with small overpotential, while the battery with the unmodified cathode/garnet interface shows no obvious plateau with large overpotential.

Declaration of interests

The authors declare that they have no known competing financial interests or personal relationships that could have appeared to influence the work reported in this paper.

The authors declare the following financial interests/personal relationships which may be considered as potential competing interests:

No potential competing interests.

Journal Pre-proof